

Distance Preserving Grid Layouts

Gladys Hilasaca and Fernando V. Paulovich



Fig. 1. DGrid layout composed of photos of famous photographers. Since similarity between images is on the eye of the viewer, we devised an application where users can create combinations of different images' features to control the semantics of the employed similarity. The widget in the bottom-right helps on controlling such combination and indicates the importance of each feature. In this case, the similarity mostly reflects the color and a little amount of information about the photographers and the objects contained in the photos. Given the high efficiency of DGrid, users can explore different combinations in real-time, rendering DGrid as a powerful mechanism for browsing and organizing image collections.

Abstract— Distance preserving visualization techniques have emerged as one of the fundamental tools for data analysis. One example are the techniques that arrange data instances into two-dimensional grids so that the pairwise distances among the instances are preserved into the produced layouts. Currently, the state-of-the-art approaches produce such grids by solving assignment problems or using permutations to optimize cost functions. Although precise, such strategies are computationally expensive, limited to small datasets or being dependent on specialized hardware to speed up the process. In this paper, we present a new technique, called Distance-preserving Grid (DGrid), that employs a binary space partitioning process in combination with multidimensional projections to create orthogonal regular grid layouts. Our results show that DGrid is as precise as the existing state-of-the-art techniques whereas requiring only a fraction of the running time and computational resources.

Index Terms—Grid Visualization, Distance Preserving Grids

1 INTRODUCTION

Distance preserving visualization techniques compose a family of strategies that seek to map data instances into graphical elements so that the pairwise distances calculated between instances are preserved as much as possible between graphical elements. Among the existing strategies, the multidimensional projections have emerged as one of the fundamental tools for data analysis [13]. Through the definition of a proper function to compute the distance between instances, projection techniques produce layouts where the dissimilarity patterns are “visible,” allowing the execution of tasks that involve the identification and analysis of distance relationships.

Despite their popularity, with applications varying from fiber tracking analysis [25] to visual text mining [5, 6, 23], projection techniques present limitations when the graphical elements are used to convey information. Given their nature of approximating distances, projection techniques tend to produce layouts with overlapped graphical elements, so suffering from occlusion problems. To address such limitation, some approaches employ post-processing strategies [11, 30] or put constraints on the projection process [24] to remove the overlapping. However, they make poor use of the visual space, creating layouts with void areas.

Aiming at making better use of the available space, distance preserving grid techniques have been devised to arrange the graphical elements into grids, using as much as possible the visual space.

Currently, the state-of-the-art approaches to produce distance-preserving grids solve assignment problems [10, 26] or use permutations to optimize cost functions [31, 32]. Although precise, such strategies are computationally expensive, limited to small datasets or being dependent on specialized hardware to speed up the process. In this paper, we introduce a novel approach, called *Distance-preserving Grid (DGrid)* that combines multidimensional projection techniques with a space-partitioning strategy to create orthogonal regular distance-preserving grids. Despite its simplicity, the quality of the produced layouts and the running times render DGrid a very attractive method for large datasets.

In summary, the main contributions of this paper are:

- A novel distance-preserving grid layout technique that presents high-quality regarding distance and neighborhood preservations while running in a fraction of the time of the current state-of-the-art techniques; and
- A framework to explore image collections that allows real-time tuning of the semantics of the similarity between images to match users expectations and the navigation of large collections into different levels of detail.

2 RELATED WORK

Different approaches have been proposed to create visual representations for conveying distance information. Dimension reduction or projection techniques are well-known examples, such as the classical scaling [35], t-SNE [36], ISOMAP [33], and LAMP [13]. Another example are the techniques that arrange geometric objects on the plane preserving similarity relations while avoiding overlaps, such as RWorle [30], IncBoard [24], ProjSnippet [11], and the UnTangle Maps [3]. It is beyond the scope of this paper to survey all possible techniques for creating distance layouts. Here we focus on strategies that arrange data into orthogonal regular grids preserving similarity relationships.

One technique that can generate distance preserving grids is the Self-Organizing Map (SOM) [14]. SOM is an unsupervised neural network that creates a discretized lower dimension representation of the data by arranging it into a two-dimensional regular spacing hexagonal or rectangular grid. The main drawback is that it can map several data instances to a single grid cell, opening spaces and overlapping instances on the composed grid [10, 26]. The same occurring to its probabilistic counterpart, the Generative Topographic Mapping (GTM) [2]. Spectral Hashing (SH) [38] can also be used (or adapted) to create distance preserving grids. SH creates hashing codes so that the Hamming distance between two codes approach the Euclidean distance between the instances they represent. Thereby, by splitting the code into bins corresponding to the rows and columns of a grid, SH codes can be used to assign data instances to grid cells preserving distances. Though a promising strategy, it suffers from the inherent problem of hashing techniques, collisions. Consequently, the produced grids also present opening spaces and overlapping instances. Our technique can also be viewed as a process to assign data instance to grid cells (indexes), but we ensure a non-overlapping constraint so that each instance is mapped to a single cell.

Another technique that can generate distance preserving grids is the NMAP [8]. NMAP is a space-filling technique that, starting from an input projection, creates rectangular arrangements through a bisecting and scaling recursive process. NMAP was designed for creating distance preserving Treemaps [29] but it can be adapted to produce grids if the rectangles' sizes (weights) are all the same. However, due to its binary partition nature, it can only build squared grids that are power-of-two. In fact, the number of rows and columns are not input parameters for NMAP, and there is no guarantee of producing orthogonal grids with cells of the same size. Our technique relies on a similar binary partition process but, different from NMAP, we use the projection to impose a distance-based ordering among the data instances. This ordering is then used to assign instances to grid cells or indexes. Our output are indexes while NMAP returns rectangles and their positions on the plane. Consequently, we can generate orthogonal grids of any dimension, covering more realistic scenarios where the dataset is not power-of-two in size.

Starting with a random assignment of the data instances to grid cells, the Self-Sorting Map (SSM) [31, 32] technique uses a permutation process, swapping instances between grid cells, aiming at maximizing a cross-correlation function between the distances among data instances and distances among the cells' positions. Since the number of possible permutations is a function of the factorial of data set size, the SSM technique searches for a locally optimal organization. In this process, the grid is split into quadrants and sub-quadrants, and swaps are performed between cells in different (sub)quadrants. Given the binary nature of this process, strategies need to be used to support non-square power-of-two grids [32]. Also, if the number of cells exceeds the number of data instances, it is not possible to control the position of the empty cells. They are (randomly) spread over the grid. In our technique the empty cells are grouped in one corner of the grid, so avoiding empty spaces inside the grid that reduces its overall quality.

The Kernelized Sorting (KS) [26] technique creates distance preserving grids finding a locally optimal solution for a quadratic assignment problem [15]. KS establishes a matrix containing the pairwise distances between the data instances and a matrix containing the pairwise distances between the grid positions. Then a permutation process is applied on the second matrix to approximate, as much as possible, the

first one, resulting in a one-to-one matching between instances and the grid cells. The IsoMatch [10] also employs an assignment strategy for constructing distance preserving grids. First, it projects the data into the plane using the ISOMAP [33] technique and builds a complete bipartite graph between the projection and grid positions. Then, using the Hungarian algorithm [16], it calculates a bipartite matching of this graph, assigning each instance to a grid position to minimize the aggregate displacement when transforming the projection positions into the grid positions. Different from the previous techniques, the KS and the IsoMatch are not limited to rectangular grids. They can create grids with arbitrary shapes. However, since they solve assignment problems, they are computationally expensive, not being able to handle large datasets or even small dataset in real-time. Our technique, although not supporting arbitrary grids, it is limited to orthogonal ones, can process much larger datasets in a fraction of the time without asking for particular hardware.

Other techniques share similarities with the approach proposed in this paper. For instance, the work by Meulemans et al. [19] positions small multiples into a grid, intentionally adding spaces to improve user perception. Another example are the well-known Cartograms [20], more specifically the Rectangular Cartograms [27, 37], that scale areas of geographical regions to rectangular shapes in proportion to some statistic, or the Tile Maps [18] that displays geographic regions as a grid of identical cell sizes. Although visually similar, they were not designed to create distance preserving grids, so out of the scope of this paper.

3 PROPOSED METHODOLOGY

The *Distance-preserving Grid (DGrid)* employs a two step approach to generate uniform grids that preserve, as much as possible, the distances relationships of a given dataset. On the first step, the data instances $\mathcal{D} = \{d_1, d_2, \dots, d_N\} \in \mathbb{R}^m$ are mapped into points on the plane using a multidimensional projection technique, obtaining their two-dimensional Cartesian Coordinates $\mathcal{P} = \{p_1 = (x_1, y_1), p_2 = (x_2, y_2), \dots, p_N = (x_N, y_N)\} \in \mathbb{R}^2$. Then, a grid $\mathcal{G} = \{g_{1,1}, g_{1,2}, \dots, g_{1,s}, \dots, g_{s,1}, g_{s,2}, \dots, g_{r,s}\}$ with r rows and s columns, where $r \times s \geq N$, is created, assigning each projected instance p_i to a grid cell $g_{p,q}$.

The reasoning behind our approach is that if the projection \mathcal{P} precisely preserves the distances relationships in \mathcal{D} , and if \mathcal{G} preserves the geometry of \mathcal{P} , \mathcal{G} will preserve the distances relationships in \mathcal{D} . Consider that \mathcal{P} has been obtained from \mathcal{D} (this is later discussed in Section 3.2). If the points in \mathcal{P} are uniformly distributed over the plane and are arranged following the number of rows and columns of the target grid, like in Figure 2(a) for a grid with 5 rows and 4 columns, the process to assign \mathcal{P} to \mathcal{G} is trivial. First, we vertically split the space into 4 partitions, with 5 instances in each, defining the column index of the instances in each partition (the horizontal numbers in Figure 2(b)). Then, we horizontally split the partitions so that each instance is placed in its partition, defining the row index of each instance (the vertical numbers in Figure 2(c)). In this example, the instance colored in red is mapped to the grid cell $g_{2,2}$, that is, the cell occupying the third row and third column.

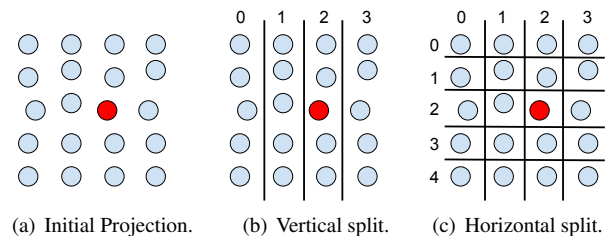


Fig. 2. Process of assigning a projection to a grid when the projection is uniformly distributed over the plane and follows the grid pattern.

In practice, the assumption that the projection is uniformly distributed over the plane and follows the grid pattern seldom holds. Seeking to approximate such constraints, we recursively bisect the projection

into non-overlapping partitions until the obtained partitions individually obey, as much as possible, such constraints. Then, (sub)grids are derived from each partition. For the first bisection, consider \mathcal{P} as the input projection, and (r, s) the dimension of the target grid. If $r > s$, we split \mathcal{P} horizontally, obtaining two partitions $\mathcal{P} = \mathcal{P}_1 \cup \mathcal{P}_2$, so that, the upper partition \mathcal{P}_1 contains enough instances to completely fill half of the desired grid, that is, $|\mathcal{P}_1| = \lceil r/2 \rceil \times s$. Otherwise, we split \mathcal{P} vertically, so that the left partition \mathcal{P}_1 contains enough instances to completely fill half of the desired grid, that is, $|\mathcal{P}_1| = r \times \lceil s/2 \rceil$. Figure 3(a) presents the result if this process is applied to a slightly modified version of Figure 2(a) to show an example where the bisectors cannot be straight lines in \mathbb{R}^2 but arbitrary curves and the simple process of Figure 2 cannot be directly used.

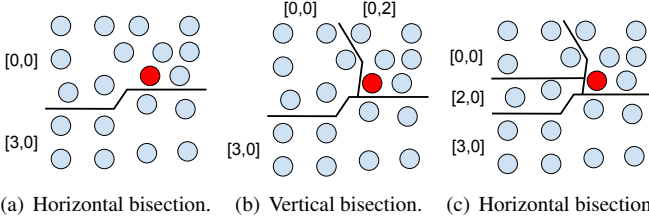


Fig. 3. Process of bisecting the projection and calculating the top-left corner indexes of the resulting grids. This process is applied until each data instance is assigned to a grid cell.

Figure 3(b) and Figure 3(c) show the bisecting process recursively applied. To compute the cells' indexes from the partitions, we calculate during the bisecting process the indexes of the top-left corner cells of each (sub)grid resulted from each partition. For instance, on Figure 3(a), the index of the top-left corner cell of the upper partition is $[0, 0]$, indicating that the grid generated from it starts at row 0 and column 0. For the lower partition, the index of the top-left corner cell is $[3, 0]$, indicating that the grid generated from it starts at row 3 and column 0. Consider that the input projection \mathcal{P} is split into \mathcal{P}_1 and \mathcal{P}_2 , where \mathcal{P}_1 is the upper partition for a horizontal cut or the left partition for a vertical cut. Also, let (i, j) be the index of the top-left corner cell of \mathcal{P} . By construction, the index of the top-left corner cell of \mathcal{P}_1 is (i, j) , and the index of \mathcal{P}_2 is $(i + \lceil r/2 \rceil, j)$ for a horizontal cut, and $(i, j + \lceil s/2 \rceil)$ for a vertical cut.

As mentioned before, this process of bisecting and calculating the top-left corner indexes are successively applied until the resulting partitions obey the uniform distribution and grid pattern constraints. However, using this as a stop criterium would penalize the computational cost of the overall algorithm since it is an $O(N^2)$ procedure for a partition containing N instances. Instead, we execute the bisecting and corner computation process until each partition contains only one instance. Notice that this returns the same grid as the process presented in Figure 2 if the input projection obeys the uniform distribution and grid pattern constraints. Therefore, it is not necessary to test if such constraints hold in any step of the algorithm, rendering a much faster and simpler process to implement.

Algorithm 1 puts all these pieces together, showing the overall process adopted by our approach to assigning a projection to a grid. The function $\text{SPLIT}_y(\mathcal{P}, k)$ performs the horizontal bisection. In this process, \mathcal{P} is sorted according to the y -coordinates (\mathcal{P} is viewed as a list), and the first k instances are assigned to \mathcal{P}_1 and the remaining to \mathcal{P}_2 . The function $\text{SPLIT}_x(\mathcal{P}, k)$ performs the vertical bisection using the same process, but sorting \mathcal{P} according to the x -coordinates. Notice that since the bisecting process always assigns to the upper and left partitions enough elements to result in a filled grid, spaces are not opened in the interior of the final grid. All empty cells are grouped on the bottom-right corner.

A different interpretation of this binary partition method is to consider it a translation process that removes void spaces so that the distribution of the projected points on the vertical and horizontal directions is as uniform as possible and follows the grid dimensions, that is, the desired number of rows and columns. Since translation is a rigid transformation that preserves relative distances, in the worst case scenario

Algorithm 1 Process of assigning a projection to a grid.

```

function DGRID( $\mathcal{G}, \mathcal{P}, (r, s), (i, j)$ )
  if  $\mathcal{P} \neq \emptyset$  then
    if  $|\mathcal{P}| = 1$  then  $\triangleright \mathcal{P}$  has one instance
       $g_{i,j} = x_0$   $\triangleright$  cell  $g_{i,j} \in \mathcal{G}$  receives the only instance in  $\mathcal{P}$ 
    else
      if  $r > s$  then
         $\mathcal{P}_1, \mathcal{P}_2 \leftarrow \text{SPLIT}_y(\mathcal{P}, \lceil r/2 \rceil \times s)$ 
        DGRID( $\mathcal{G}, \mathcal{P}_1, (\lceil r/2 \rceil, s), (i, j)$ )
        DGRID( $\mathcal{G}, \mathcal{P}_2, (r - \lceil r/2 \rceil, s), (i + \lceil r/2 \rceil, j)$ )
      else
         $\mathcal{P}_1, \mathcal{P}_2 \leftarrow \text{SPLIT}_x(\mathcal{P}, r \times \lceil s/2 \rceil)$ 
        DGRID( $\mathcal{G}, \mathcal{P}_1, (r, \lceil s/2 \rceil), (i, j)$ )
        DGRID( $\mathcal{G}, \mathcal{P}_2, (r, s - \lceil s/2 \rceil), (i, j + \lceil s/2 \rceil)$ )
      end if
    end if
  end if
end function

```

half of the distance relationships are fully kept when a projection is bisected. Typically, more than that is preserved, so that the geometry of \mathcal{P} is preserved, up to an extent, by \mathcal{G} , and, consequently, the produced grid preserves the distances relationships in \mathcal{D} .

3.1 Grid Dimension

The process of assigning a projection to a grid defined in the previous section is very flexible. Since it focuses on splitting the partitions considering the number of rows and columns, instead of the number of data instances, it is not limited to any particular grid shape. The only constraint is that the number of grid cells should be larger or equal to the number of data instances, that is, $r \times s \geq N$.

In this paper, we allow the control of the grid shape by defining its aspect-ratio Δ . Here, the aspect-ratio can be the ratio between the number of rows and the number of columns of the final grid, or the ratio between the height and width of the visual space. Given Δ , the target grid dimension is calculated as

$$\begin{aligned} r &= \lfloor \sqrt{N * \Delta} \rfloor \\ s &= \lceil N / r \rceil \end{aligned} \quad (1)$$

If $\Delta = 1$, the resulting grid will as square as possible. If $0 < \Delta < 1$, the resulting grid will present more columns than rows. The opposite if $\Delta > 1$.

3.2 Projecting the Dataset

We aim to preserve on the produced grid the distance relationships of a given dataset \mathcal{D} by assigning similar data instances to close grid cells, and dissimilar ones to far apart cells. In this context, the projection \mathcal{P} plays a central role since it guides the grid geometry. Therefore, \mathcal{P} should preserve, as much as possible, the distance relationships in \mathcal{D} . In the current literature, there are several multidimensional projection techniques to derived \mathcal{P} from \mathcal{D} . Typically, the most precise techniques, such as the classical multidimensional scaling [35] or the t-SNE [36], are computationally expensive, whereas the less precise out-of-sample methods, such as LAMP [13] or the PLMP [22], can handle very large datasets in a reasonable amount of time. Thereby, the choice of what technique to use rely mostly on the tradeoff between the size of the dataset and the desired precision.

4 EVALUATION AND COMPARISON

4.1 Quantitative Analysis

In this section we present a quantitative evaluation of the *Distance-preserving Grid (DGrid)* technique, comparing it against the state-of-the-art in distance preservation grid techniques, viz., Kernelized Sorting (KS) [26], Self-Sorting Map (SSM) [32], and IsoMatch [10]. In this comparison we use three different quality metrics, k -neighborhood preservation index [9], cross-correlation [32], and energy function [10].

The k -neighborhood preservation index was originally developed to evaluate projections, but here we use it to measure how much the neighborhood in the dataset \mathcal{D} is preserved in the grid \mathcal{G} . It is calculated as

$$NP_k = \frac{1}{N} \sum_i \frac{N_{k_i}^{\mathcal{D}} \cap N_{k_i}^{\mathcal{G}}}{k} \quad (2)$$

where $N_{k_i}^{\mathcal{D}}$ is the set containing the indexes of the k -nearest neighbors of d_i in \mathcal{D} , and $N_{k_i}^{\mathcal{G}}$ is the set containing the indexes of the k -nearest neighbors of g_i in \mathcal{G} . NP_k ranges in $[0, 1]$, the larger the value the better the result. The cross-correlation measures how well the placements of the data instances in the grid correlate to the dissimilarities among them, given by

$$CC = \sum_i \sum_j \frac{(\lambda(g_i, g_j) - \bar{\lambda})(\delta(d_i, d_j) - \bar{\delta})}{\sigma_\lambda \sigma_\delta} \quad (3)$$

where $\delta(d_i, d_j)$ is the dissimilarity between pairs of instances, $\lambda(g_i, g_j)$ is the distance between the cells the instances are assigned to, $\bar{\lambda}$ is the mean distance between any two cells, $\bar{\delta}$ is the mean distance between any two pairs of instances, and σ_λ and σ_δ are the corresponding standard deviation. The cross-correlation ranges in $[-1, 1]$, the larger the better. In this paper, we normalize the cross-correlation in $[0, 1]$ using $CC' = (CC + 1)/2$ to easier the comparison among the different metrics. Finally, the energy function measures how well the pairwise distances between the data instances are preserved by the corresponding distances in the grid. This function is computed as

$$E_p = \left(\sum_i \sum_j \frac{|c \cdot \delta(d_i, d_j) - \lambda(g_i, g_j)|^p}{\sum_r \sum_s \lambda(g_r, g_s)^p} \right)^{\frac{1}{p}} \quad (4)$$

where p defines the employed norm, and c is a scaling constant (see [10] for more details). As suggested in [10], we set $p = 1$ since it favors solutions which preserve the smaller distances more than the larger ones. Also, we invert the original equation using $E'_p = 1 - E_p$ so that it ranges in $[0, 1]$ with larger values rendering better results.

For the tests we have selected all datasets from the *UCI Machine Learning Repository* [17] with real-valued attributes and sizes varying between 100 and 2,500 instances, allowing the comparison of the techniques in different scenarios. We only get real-valued datasets so that (Euclidean) distances can be properly calculated, and we limited their sizes due to the high computational complexities and running times of KS and IsoMatch. Also, we have discarded the datasets with missing values, resulting in 38 datasets. The first part of Table 1 details these datasets, presenting their names, sizes, and number of dimensions. For all tests, we have normalized the datasets so that the columns (attributes) have zero mean and standard deviation equals to one. All the results were generated in an Intel Core *i7 CPU@2.8GHz*, with 16GB of RAM. For the SSM, KS, and IsoMatch techniques we used the original codes, made available by the authors.

Figure 4 presents boxplots summarizing the results of each technique considering all the 38 datasets. For the DGrid, we report results using the t-SNE and LAMP techniques to generate the input projections. Although the IsoMatch originally employs the ISOMAP as input, we also report results using the t-SNE and LAMP, so it is possible to compare the DGrid and the IsoMatch isolating the projection contribution to the quality of the produced results. The DGrid, IsoMatch, and KS techniques are deterministic, so we only run each technique once for each dataset. Given the random initialization of the SSM technique, we run it 30 times for each dataset. In Figure 4, the boxplots in red represent the results of the projections (LAMP and t-SNE) used as input by DGrid and IsoMatch techniques. They serve only as baselines to show the correlation between projection quality and grid quality. Notice that, the drop in precision between the projections and the produced grids is expected since the techniques we use do not create uniformly distributed projections (see Section 3). Also note that direct comparisons only make sense among grid layouts, not among grids and projections.

Table 1. Datasets employed in the evaluations. We have selected all datasets from the *UCI Machine Learning Repository* with real-valued attributes and sizes up to a limit, allowing the comparison of the techniques in different scenarios.

Name	Size	Dimensions
Concrete Slump Test	103	10
Breast Tissue	106	10
LSVT Voice Rehabilitation	126	309
Iris	150	4
Urban Land Cover	168	148
Planning Relax	182	13
Parkinsons	197	23
Connectionist Bench	208	60
Seeds	210	7
Glass Identification	214	10
Yacht Hydrodynamics	308	7
Vertebral Column	310	6
Ecoli	336	8
Leaf	340	16
Libras Movement	360	91
PEMS	440	138,672
Forest Fires	517	11
Vowel Recognition	528	10
Istanbul Stock Exchange	536	8
Climate	540	18
WDBC	569	32
DrivFace	606	6,400
Hill-Valley	606	100
Blood Transfusion	748	5
Gene Expression	801	20,531
Arcene	900	10,000
MicroMass	931	1,300
Cloud	1,024	10
Concrete Compressive Strength	1,030	9
Geographical Original of Music	1,059	68
Banknote Authentication	1,372	5
Yeast	1,484	8
Airfoil Self-Noise	1,503	5
Plant species leaves	1,600	64
Drug Consumption	1,885	32
Cardiotocography	2,126	23
Image Segmentation	2,100	19
Statlog (Image Segmentation)	2,310	19
HTRU2	17,898	9
Default of credit card	30,000	23
Online News Popularity	39,644	61
Facebook Comments	40,949	54
Tamilnadu Electricity Board	45,781	4
Sensorless Drive Diagnosis	58,509	49
Corel Image Features	68,040	89
Blog Feedback	56,497	281
FMA: A Dataset For Music Analysis	106,574	518
MiniBooNE Particle Identification	130,065	50

Regarding the k -neighborhood preservation index, Figure 4(a), the best result was attained by the DGrid with t-SNE as input ($\overline{NP} = 0.52$), better than the other more costly counterparts, IsoMatch ($\overline{NP} = 0.36$) and KS ($\overline{NP} = 0.50$). DGrid presents not only the largest mean but also the smallest spread regarding the best and worst results. Comparing the different flavors of DGrid, the results produced using the t-SNE are also considerably superior than the results produced using the LAMP. This is an expected outcome since the formulation of t-SNE favors the preservation of small neighborhoods instead of a global distance preservation as conveyed by the LAMP, which is confirmed by the boxplots of the projections in red. This indicates the impact of the input projection to the produced grid, and also shows that our strategy for assigning the projection to grid cells satisfactorily preserves the input geometry. In this example, we approximate the neighborhood size k to 5% of the dataset size, setting $k = (\lfloor \sqrt{0.05 * N} \rfloor)^2$. We use this approximation instead of 5% to match the grid topology when calculating the neighborhoods.

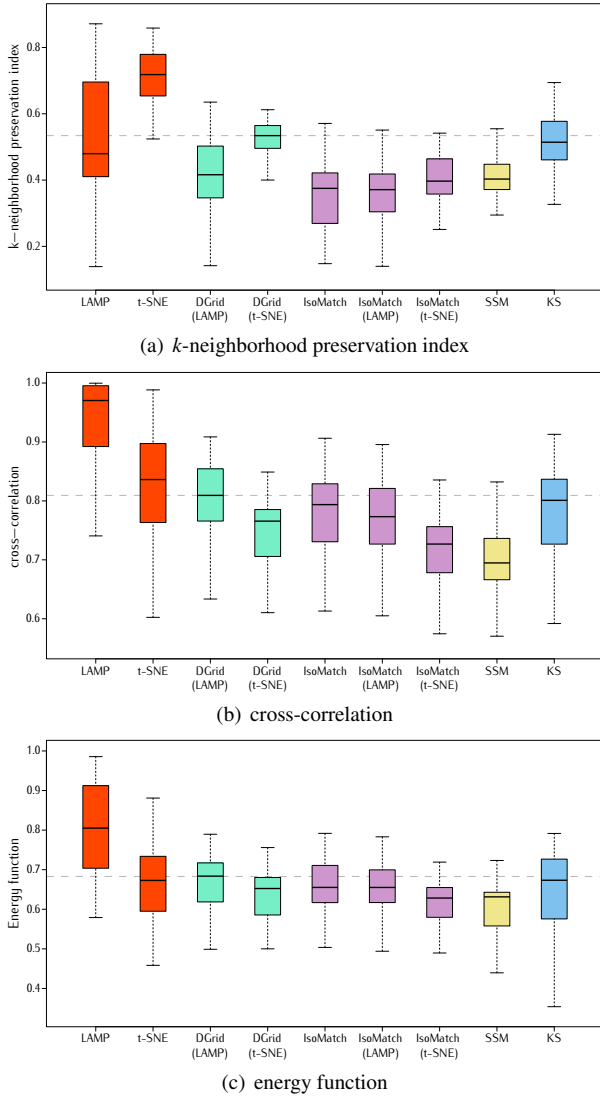


Fig. 4. Boxplots of k -neighborhood preservation index, cross-correlation, and energy function. In all these aspects, the DGrid surpass (on average) current state-of-the-art techniques, indicating its quality on preserving distance relationships. The boxplots in red summarize the results of the input projection and serve as baselines to show the correlation between projections and grid properties. They are not intend for direct comparisons.

Figure 4(b) shows the cross-correlation results. On average, DGrid with LAMP ($\overline{CC^T} = 0.80$) presents better results than IsoMatch ($\overline{CC^T} = 0.78$) and KS ($\overline{CC^T} = 0.78$), with a smaller spread regarding the best and worst results. Different from the k -neighborhood preservation index, which is a local measure, the cross-correlation is global, explaining why the results considering LAMP as input are better than the ones considering the t-SNE, which is also confirmed by the projection boxplots in red. This renders exceptional flexibility to our technique since it allows selecting a projection technique that fulfills specific needs, considering different global or local geometry properties, generating grids that satisfactorily preserve them.

The quality of our approach is also confirmed by the energy function metric (Figure 4(c)). The DGrid with the LAMP ($\overline{E^T_p} = 0.65$) again outperforms the other techniques, IsoMatch ($\overline{E^T_p} = 0.63$) and KS ($\overline{E^T_p} = 0.63$). Since the energy function is a global measure, the LAMP technique presents better results than the t-SNE (see the red boxplots), which reflects in the produced grids. In [10], the authors show that the energy function strongly correlates with human performance in search tasks, pointing that this is a good measure of grid organization. The

same holds for the cross-correlation measure. Therefore, the attained results provide evidence to place the combination of DGrid with the LAMP as one of the best choices for tasks that involve the analysis of similarity relationships based on grids.

To complement the statistical analysis conveyed by the boxplots, providing more detailed information, we show in Figures 5, 6, and 7 the resulting grids for some selected datasets. Aiming at showing different aspects of each technique, we choose datasets with varied distance distributions, from a dataset with most instances similar among themselves (Forest) to a dataset with most instances dissimilar among themselves (MicroMass). In these figures, the cells are colored according to different quality metrics calculated for each cell. The cells colored in black are empty. They exist because we have more cells than instances in these examples. Notice that the DGrid, KS, and IsoMatch place all empty cells on the grid borders whereas the SSM open spaces inside the grid. The quality metric values are shown below each grid, and the best results are highlighted using a bold font. Although KS is marginally better in one case and presents the same quality as DGrid in other cases, it is an $O(N^3)$ technique and cannot address problems involving large datasets. DGrid is much less expensive (see Section 6) so not only small examples can be processed in a fraction of the time but also it can address larger problems that neither KS nor IsoMatch are capable of.

Regarding the k -neighborhood preservation index grids (Figure 5), the KS and the DGrid with t-SNE, which attained the best results on average (see Figure 4), do not present spots concentrating bad quality cells, the error is uniformly spread over the grid. Conversely, SSM tends to group the bad quality cells close to the empty cells, showing their negative impact on the produced layouts. The cross-correlation grids (Figure 6) report an intriguing pattern produced by all techniques. For the Forest dataset, there is a clear spot with bad quality cells, concentrated in the border of two different regions. A close examination explains the reason. Since the Forest dataset is composed of two very distinct groups of instances, approaching them in the produced layout increases the error in the border cells, an inevitable aspect of grid layouts. The energy function grids (Figure 7) also present an unusual pattern regarding the Forest dataset. The two different groups of instances can also be identified, but in these grids, the larger group presents significant worse results if compared to the smaller one (compare with Figure 6). In this case, the problem is related to the size of the groups. Since one group is much larger than the other, considering the groups individually defines two different scenarios regarding distance distribution. For the smaller group, most instances are dissimilar between themselves, but for the larger, most instances are similar between themselves. Since the energy function is global and measures the distance preservation, the differences in distribution affect the quality of the grid cells.

Given the process we develop to derive grids from projections, our approach can obtain better results if the number of rows and columns, controlled by Δ , is defined considering the distribution of the input projections. Figure 8 shows the impact of varying Δ into the quality of the produced grids. To have better control of this test, we artificially generate a projection with three times more points in the vertical direction than in the horizontal direction. As expected, the best results are attained when $\Delta = 3$ (the dashed line). In all examples in this section we have used squared grids, setting $\Delta = 1$. Since most techniques we are comparing to do not depend on projections, we prefer to set a fixed value instead of using the best possible value of Δ to not bias the evaluation favoring our approach.

Finally, we have compared DGrid with SSM regarding the running times. We have removed the other techniques from this comparison since they are computationally expensive, not capable of processing large datasets. In this test we have selected 10 datasets from the *UCI Machine Learning Repository*, varying the sizes up to 130,000 instances. The employed datasets are detailed in the second part of Table 1. Figure 9 summarizes the results. To allow a fair comparison, DGrid and SSM are both implemented in Java. Besides the boxplots for the DGrid and the SSM techniques, the figure shows individual boxplots for the projection and the grid assignment steps. In this example, we are using the LAMP to project the data. On average, the

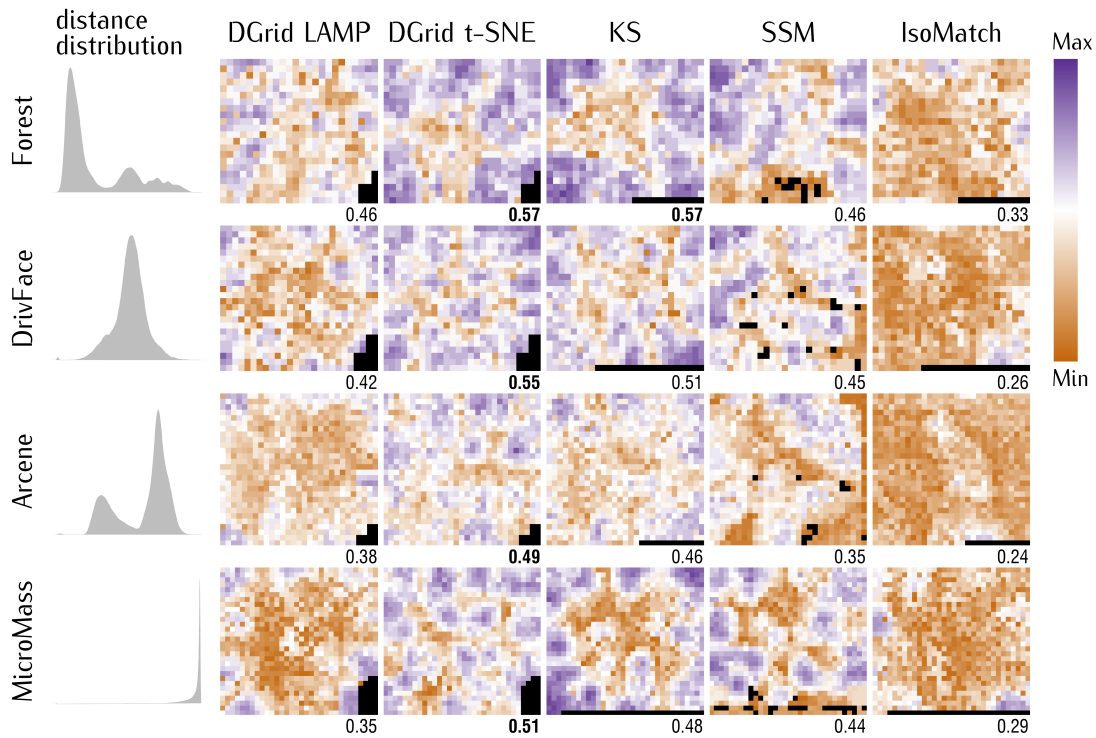


Fig. 5. Resulting grids colored according to the **k-neighborhood preservation index**. SSM technique groups bad quality cells close to the empty cells, showing the negative impact of empty spots on the produced layouts.

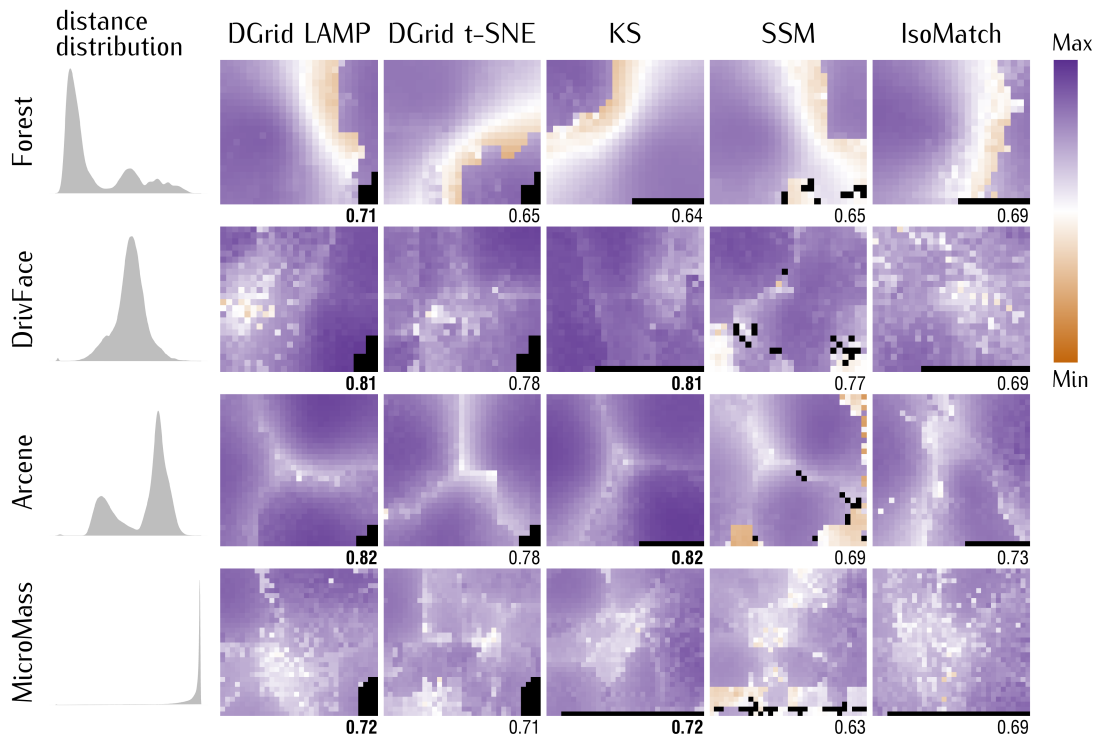


Fig. 6. Resulting grids colored according to the **cross-correlation**. Cross-correlation is global measure, so the use of a global projection technique (LAMP) as input resulted in better grids in that aspect. This renders exceptional flexibility to our approach since it allows selecting a projection technique that fulfills specific geometry properties, generating grids that satisfactorily preserve them.

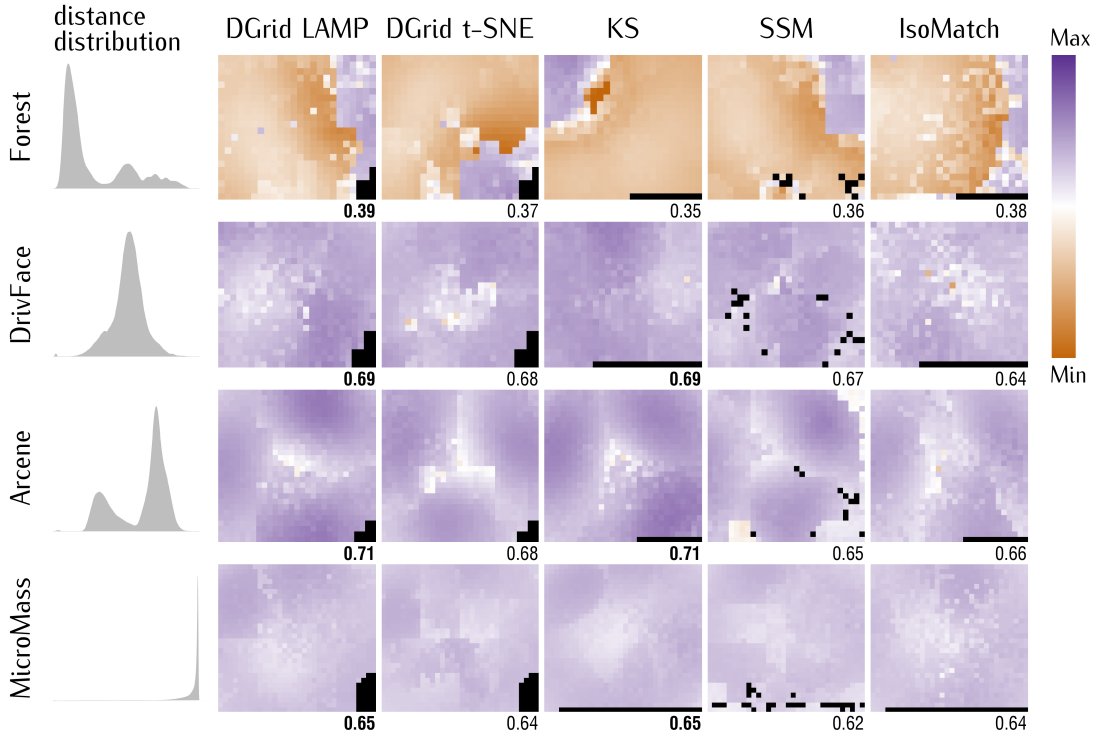


Fig. 7. Resulting grids colored according to the **energy function**. The energy function strongly correlates with human performance in search tasks, placing DGrid among the best choices for tasks that involve the analysis of similarity relationships based on grids.

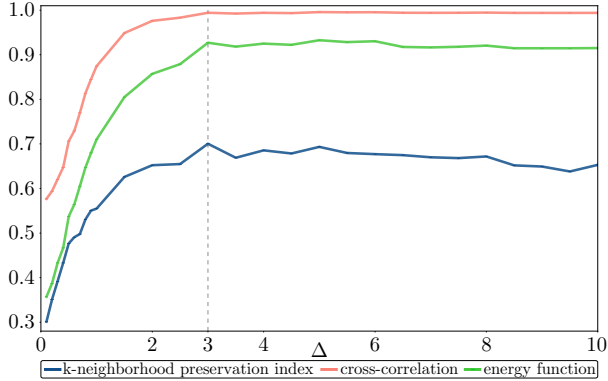


Fig. 8. Impact of varying the grid dimensions to the quality of the produced layouts. The best results are attained when the grid dimensions are related to the distribution of the input projection.

DGrid is almost two orders of magnitude faster than the SSM, but better results can be obtained if a faster projection technique is employed (the projection step dominates the process). Considering the tested techniques, DGrid presents the best tradeoff between running times and quality of the produced grids, placing it among the state-of-the-art techniques for generating distance preserving grids from large datasets.

4.2 Qualitative Analysis

5 APPLICATION

Exploring image collections have been one of the main applications for distance preserving grids, with a positive impact on image retrieval tasks [28]. In this section, we present a strategy using DGrid to explore photo collections that allow users to control the semantics of the similarity between images and to navigate collections into different levels of detail.

Figure 10 overviews our approach. First, the photo collection is processed to extract different sets of features f_1, f_2, \dots, f_k , representing different elements of a photo, such as colour, the presence of objects,

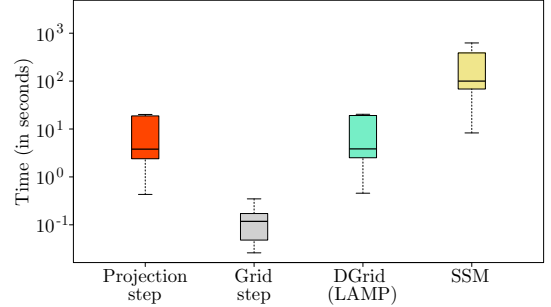


Fig. 9. Running times boxplots. DGrid is almost two orders of magnitude faster than the SSM technique, and the projection phase dominates its running times. We have removed the other technique from this comparison since they are not capable of processing large datasets.

and so on. From each set of features we extract samples of photos s_1, s_2, \dots, s_k that are joined to compose our complete sample $S = s_1 \cup s_2 \cup \dots \cup s_k$. For sampling, we use the k-means technique to cluster the data, getting the medoid of each cluster as a sample. By getting samples using the different set of features, we seek to guarantee that we have images that contain the different traits captured by the different features. After that, projections p'_1, p'_2, \dots, p'_k are generated considering the images in S but using the different types of features f'_1, f'_2, \dots, f'_k . The input projection for building the sample grid is then created as a convex combination of these projections, that is, $P' = \alpha_1 p'_1 + \alpha_2 p'_2 + \dots + \alpha_k p'_k$, where $\sum \alpha_i = 1$. By changing $\alpha_1, \alpha_2, \dots, \alpha_k$ users can control the contribution of each different projection to the complete projection, implicitly controlling the importance of each type of feature to the semantics of the employed similarity. After defining the most appropriated weights for the convex combination, the projection P used to create the complete grid with all photos is defined as a combination of projections p_1, p_2, \dots, p_k of the complete dataset but considering the different features, that is, $P = \alpha_1 p_1 + \alpha_2 p_2 + \dots + \alpha_k p_k$.

Here, we use the Photographer dataset [34], composed of 180,193 photos taken by 41 well-known photographers. We extract 4 different

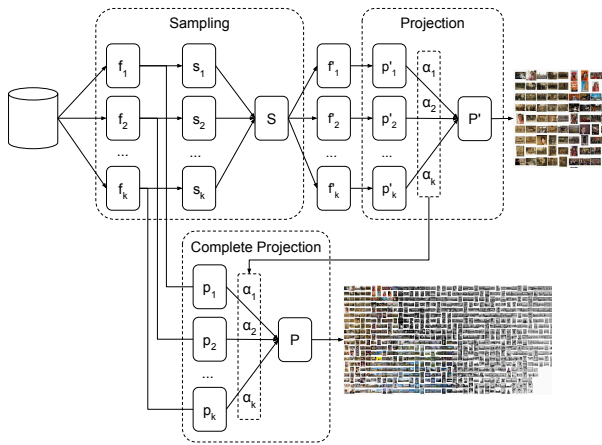


Fig. 10. Overview of our strategy to compose a photo grid that allows users to control the semantics of the similarity between images. Based on a small sample, users can interactively combine different features seeking for the combination that best approaches his/her point of view regarding similarity. This combination is then propagated to the entire dataset to compose the complete grid which can then be explored into different levels of detail.

sets of features from this dataset, representing: (1) color, using LaB color features; (2) texture, using Gabor filters [4]; (3) borders, using the HoG technique [7]; and (4) the presence of objects, using a pre-trained convolutional neural network, called CaffeNet [12], that classifies images into 1,000 different object categories. Also, we create a set of features to represent the similarity between photographers using an external source. We download Wikipedia articles about each photographer and construct a bag-of-words vector representation for each. All photos of the same photographer are then represented by his/her vector representation. Consequently, the similarity among photos is defined as the similarity between texts describing the photographers.

In this paper, to create the sample S we get 200 photos of each different set of features, ensuring we have at least 5 photos of each photographer (800 photos in total). Figure 1 shows the resulting sample grid. In this grid, the similarity mostly reflects the color and a little amount of information about the photographers and the objects contained in the photos. To visually support this combination, we develop a widget, shown in the bottom-right of the figure, inspired by the idea presented in [21]. Using this widget, $\alpha_1, \alpha_2, \dots, \alpha_k$ are defined based on the closeness of the “orange” dial and the anchors representing each feature. To help the perception of the weights, we change the transparency level of the anchors and fonts accordingly. Since the similarity between images is on the eye of the viewer, allowing users to control the semantics of the employed similarity based on combinations of different features renders a powerful mechanism.

We are combining projections instead of features to allow a real-time exploration of the different combinations. In this strategy, projections for each set of features are calculated once. Only the grid is derived when the combination is changed. Since grids are built from projections almost instantly for reasonable amounts of data (see Figure 9), our approach allows the exploration in interactive rates. If we opt to combine features, a projection should be produced after changing a combination, and, currently, there are no good quality projection techniques that are fast enough to attain interactive rates. Notice that, this application is only possible given the high efficiency of DGrid to derive grids in real-time, a trait not found in the current state-of-the-art techniques in distance preserving grid layouts.

Once the proper combination has been defined from the users’ point of view, a grid representing the complete photo collection is constructed. Considering the dataset size and setting $\Delta = 11/8.5$ to match the aspect ratio of the visual area (paper size), the resulting photo grid has 482 rows and 374 columns. Since this is too much information to present at once, we allow the grid compression. In this process, we convolute the grid with a $R \times S$ mask merging the covered cells into one single

cell, thus dividing the number of rows by R and the number of columns by S . In the compact layout, the cells are represented by the photo closest to the center of the $R \times S$ mask. Figure 11 presents the resulting compressed photo grid. In this example, we use a 5×5 mask, resulting in a grid with 96 rows and 75 columns.

The mask $R \times S$ defines the level of detail of the compact representation. Changing its size allows the navigation of the photo collection into different levels of abstraction, from a coarse representation to a more detail view. Another possibility of navigation is to allow users to select a particular photo, expanding the compressed grid to show all the photos it represents. In this case, by expanding all the cells belonging to the same row or same column of the selected photo, we define a multilevel process that preserves the context. In [10] a similar application was presented. However, they use a hierarchical clustering approach to group the instances, showing representatives of the groups. The user can then navigate by clicking on the representatives, displaying new grids containing the elements (or representatives) inside the groups. Therefore, losing the context whenever a zoom in operation is executed.

6 DISCUSSION AND LIMITATIONS

The space partition strategy presented in Algorithm 1 shares similarities with the kd-tree technique [1]. In both cases, the recursive process of bisecting the space into partitions and sub-partitions constructs complete binary trees. The difference is that the kd-tree only considers the spatial position of the points in this process whereas our approach incorporates the number of rows and columns to it. As a result, our technique can create grids with an arbitrary number of rows and columns while the kd-tree can only create squared grids that are power-of-two [32]. The same applying to the NMAP technique [8] as discussed in Section 2.

Regarding the computational complexity, the DGrid has two distinct steps. The projection and the space partition. Different techniques can be used in the first step, with different complexities. Here we use the t-SNE which is $O(N^2)$ and the LAMP which is $O(\min\{m^2 N^{\frac{3}{2}}, mN^2\})$, where m is the number of dimensions of the dataset. Recalling that every time a partition is bisected, its instances are sorted according to the x or y coordinates. If an $O(N \log N)$ sorting algorithm is used, the computational complexity of the space partition step is $O(N \log^2 N)$. Therefore, the overall computational complexity is dominated by the projection process, which is confirmed by the running times (see Figure 9). If a faster approach is required, changing the projection technique is an option, for instance, PLMP [22] is $O(N)$, but probably the quality of the obtained grids will be penalized.

The way DGrid was conceived only allows it to generate orthogonal regular grids. KS and IsoMatch are more flexible. Since they are based on assignment processes, they can map data instances into non-orthogonal domains. However, they are computationally expensive, $O(N^3)$. For orthogonal grids the DGrid is much faster, attaining similar or even better results considering different quality metrics, rendering DGrid a very attractive technique for processing large datasets.

Finally, in our space partition process, we consider a simple splitting method, dividing the space so that the resulting partitions contain approximately half of the instances. Defining a better way to partition the space is an aspect that deserves to be investigated more deeply, for instance, guiding the partition according to the distribution of the points on the plane. However, finding the best partitioning considering both the data distribution and the grid dimension constraint is not a trivial task.

7 CONCLUSION

In this paper, we proposed a novel approach for generating grid layouts that preserve distance information, called *Distance-preserving Grid (DGrid)*. DGrid is a two-step approach that combines a projection technique with an assignment strategy to create orthogonal regular grids. The set of comparisons we provide shows that DGrid outperforms the existing state-of-the-art techniques considering different quality metrics, being almost two orders of magnitude faster than the fastest existing technique. The quality of the produced layouts combined with the low

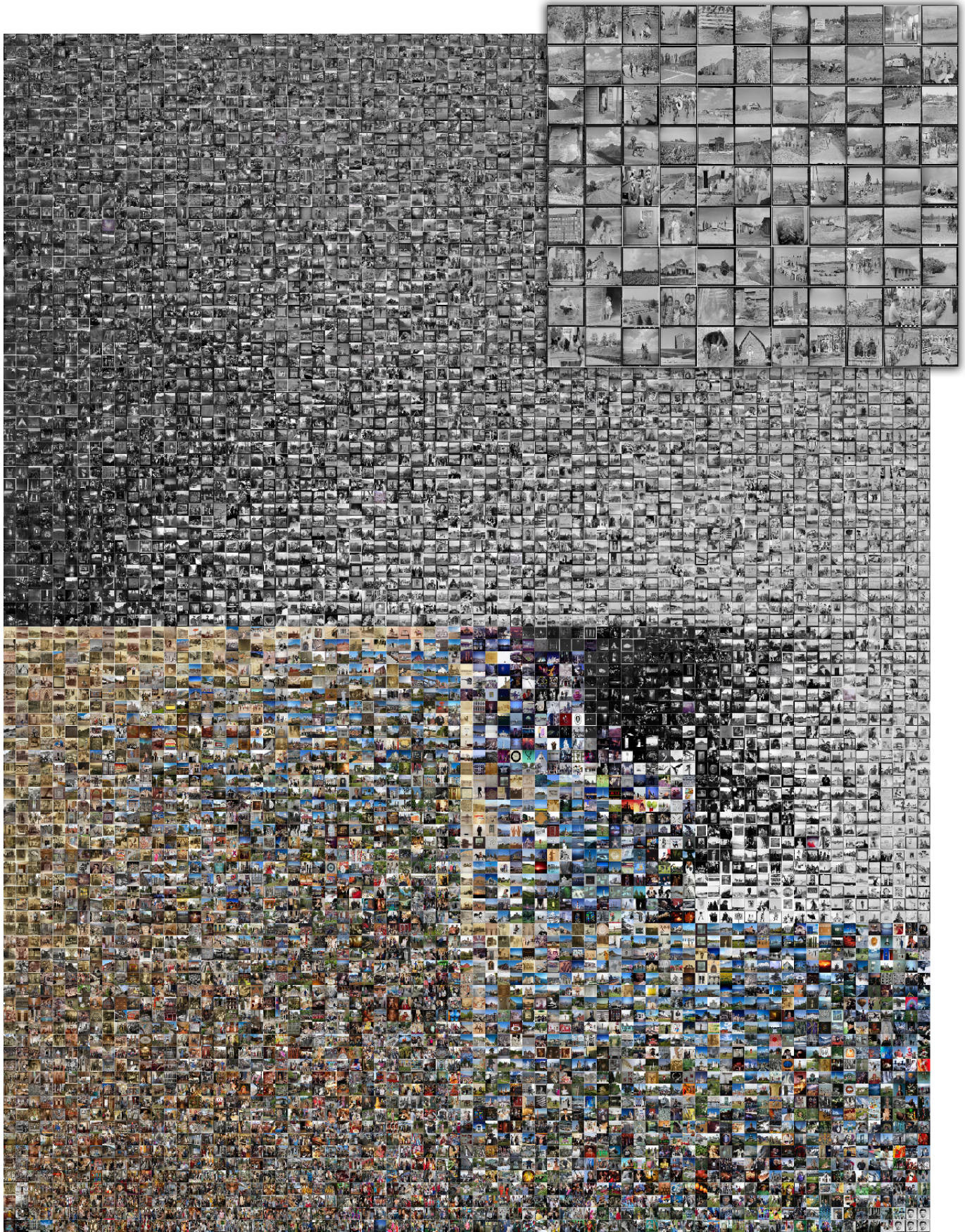


Fig. 11. Photo grid of the Photographers dataset. Since a considerably larger weight is assigned to the color features (see Figure 1), a clear global separation between gray and colored photos can be observed. We also add the presence of objects and photographer style into the feature combination, so locally these features influence, up to and extent, the grid organization as noted in the zoom in part of the top-right corner.

computational cost render DGrid one of the most attractive methods for generating distance preserving grid layouts.

REFERENCES

- [1] J. L. Bentley. Multidimensional binary search trees used for associative searching. *Commun. ACM*, 18(9):509–517, Sept. 1975. doi: 10.1145/361002.361007
- [2] C. M. Bishop, M. Svensén, and C. K. I. Williams. Gtm: The generative topographic mapping. *Neural Computation*, 10(1):215–234, Jan 1998. doi: 10.1162/089976698300017953
- [3] N. Cao, Y. R. Lin, and D. Gotz. Untangle map: Visual analysis of probabilistic multi-label data. *IEEE Transactions on Visualization and Computer Graphics*, 22(2):1149–1163, Feb 2016. doi: 10.1109/TVCG.2015.2424878
- [4] L. Chen, G. Lu, and D. Zhang. Effects of different gabor filter parameters on image retrieval by texture. In *Proceedings of the 10th International Multimedia Modelling Conference, MMM '04*, pp. 273–. IEEE Computer Society, Washington, DC, USA, 2004.
- [5] Y. Chen, J. Hua, M. Dong, and L. Wang. Exemplar-based visualization of large document corpus (infovis2009-1115). *IEEE Transactions on Visualization & Computer Graphics*, 15:1161–1168, 09 2009. doi: 10.1109/TVCG.2009.140
- [6] W. Cui, Y. Wu, S. Liu, F. Wei, M. X. Zhou, and H. Qu. Context-preserving, dynamic word cloud visualization. *IEEE Comput. Graph. Appl.*, 30(6):42–53, Nov. 2010. doi: 10.1109/MCG.2010.102
- [7] N. Dalal and B. Triggs. Histograms of oriented gradients for human detection. In *In CVPR*, pp. 886–893, 2005.
- [8] F. S. L. G. Duarte, F. Sikansi, F. M. Fatore, S. G. Fadel, and F. V. Paulovich. Nmap: A novel neighborhood preservation space-filling algorithm. *IEEE Transactions on Visualization and Computer Graphics*, 20(12):2063–2071, Dec 2014. doi: 10.1109/TVCG.2014.2346276
- [9] S. G. Fadel, F. M. Fatore, F. S. Duarte, and F. V. Paulovich. Loch: A neighborhood-based multidimensional projection technique for high-dimensional sparse spaces. *Neurocomputing*, 150(Part B):546 – 556, 2015. doi: 10.1016/j.neucom.2014.07.071
- [10] O. Fried, S. DiVerdi, M. Halber, E. Sizikova, and A. Finkelstein. Isomatch: Creating informative grid layouts. *Comput. Graph. Forum*, 34(2):155–166, May 2015. doi: 10.1111/cgf.12549
- [11] E. Gomez-Nieto, F. S. Roman, P. Pagliosa, W. Casaca, E. S. Helou, M. C. F. de Oliveira, and L. G. Nonato. Similarity preserving snippet-based visualization of web search results. *IEEE Transactions on Visualization and Computer Graphics*, 20(3):457–470, March 2014. doi: 10.1109/TVCG.2013.242
- [12] Y. Jia, E. Shelhamer, J. Donahue, S. Karayev, J. Long, R. Girshick, S. Guadarrama, and T. Darrell. Caffe: Convolutional architecture for fast feature embedding. In *Proceedings of the 22Nd ACM International Conference on Multimedia, MM '14*, pp. 675–678. ACM, New York, NY, USA, 2014. doi: 10.1145/2647868.2654889
- [13] P. Joia, D. Coimbra, J. A. Cuminato, F. V. Paulovich, and L. G. Nonato. Local affine multidimensional projection. *IEEE Transactions on Visualization and Computer Graphics*, 17(12):2563–2571, Dec. 2011. doi: 10.1109/TVCG.2011.220
- [14] T. Kohonen. *Neurocomputing: Foundations of research*. chap. Self-organized Formation of Topologically Correct Feature Maps, pp. 509–521. MIT Press, Cambridge, MA, USA, 1988.
- [15] T. C. Koopmans and M. Beckmann. Assignment problems and the location of economic activities. *Econometrica*, 25(1):53–76, 1957.
- [16] H. W. Kuhn. The hungarian method for the assignment problem. *Naval Research Logistics Quarterly*, 2(1-2):83–97, 1955. doi: 10.1002/nav.3800020109
- [17] M. Lichman. UCI machine learning repository, 2013.
- [18] G. McNeill and S. A. Hale. Generating tile maps. *Comput. Graph. Forum*, 36(3):435–445, June 2017. doi: 10.1111/cgf.13200
- [19] W. Meulemans, J. Dykes, A. Slingsby, C. Turkay, and J. Wood. Small multiples with gaps. *IEEE Transactions on Visualization and Computer Graphics*, 23(1):381–390, Jan 2017. doi: 10.1109/TVCG.2016.2598542
- [20] S. Nusrat and S. Kobourov. The state of the art in cartograms. *Computer Graphics Forum*, 35(3):619–642, 2016. doi: 10.1111/cgf.12932
- [21] P. Pagliosa, F. V. Paulovich, R. Minghim, H. Levkowitz, and L. G. Nonato. Projection inspector: Assessment and synthesis of multidimensional projections. *Neurocomputing*, 150, Part B:599–610, 2015. doi: 10.1016/j.neucom.2014.07.072
- [22] F. V. Paulovich, C. T. Silva, and L. G. Nonato. Two-phase mapping for projecting massive data sets. *IEEE Transactions on Visualization and Computer Graphics*, 16(6):1281–1290, Nov. 2010. doi: 10.1109/TVCG.2010.207
- [23] F. V. Paulovich, F. M. B. Toledo, G. P. Telles, R. Minghim, and L. G. Nonato. Semantic wordification of document collections. *Comput. Graph. Forum*, 31(3pt3):1145–1153, June 2012. doi: 10.1111/j.1467-8659.2012.03107.x
- [24] R. D. Pinho, M. C. Oliveira, and A. Andrade Lopes. An incremental space to visualize dynamic data sets. *Multimedia Tools Appl.*, 50(3):533–562, Dec. 2010. doi: 10.1007/s11042-010-0483-5
- [25] J. Poco, D. M. Eler, F. V. Paulovich, and R. Minghim. Employing 2d projections for fast visual exploration of large fiber tracking data. *Computer Graphics Forum*, 31(3pt2):1075–1084, 2012. doi: 10.1111/j.1467-8659.2012.03100.x
- [26] N. Quadrianto, A. J. Smola, L. Song, and T. Tuytelaars. Kernelized sorting. *IEEE Transactions on Pattern Analysis and Machine Intelligence*, 32(10):1809–1821, Oct 2010. doi: 10.1109/TPAMI.2009.184
- [27] E. Raisz. The rectangular statistical cartogram. *Geographical Review*, 24(2):292–296, 1934.
- [28] K. Schoeffmann and D. Ahlstrom. Similarity-based visualization for image browsing revisited. In *2011 IEEE International Symposium on Multimedia*, pp. 422–427, Dec 2011. doi: 10.1109/ISM.2011.76
- [29] B. Shneiderman. Tree visualization with tree-maps: 2-d space-filling approach. *ACM Trans. Graph.*, 11(1):92–99, Jan. 1992. doi: 10.1145/102377.115768
- [30] H. Strobel, M. Spicker, A. Stoffel, D. Keim, and O. Deussen. Rolled-out wordles: A heuristic method for overlap removal of 2d data representatives. *Computer Graphics Forum*, 31(3pt3):1135–1144, 2012. doi: 10.1111/j.1467-8659.2012.03106.x
- [31] G. Strong and M. Gong. Data organization and visualization using self-sorting map. In *Proceedings of Graphics Interface 2011, GI '11*, pp. 199–206. Canadian Human-Computer Communications Society, School of Computer Science, University of Waterloo, Waterloo, Ontario, Canada, 2011.
- [32] G. Strong and M. Gong. Self-sorting map: An efficient algorithm for presenting multimedia data in structured layouts. *Trans. Multi.*, 16(4):1045–1058, June 2014. doi: 10.1109/TMM.2014.2306183
- [33] J. B. Tenenbaum, V. d. Silva, and J. C. Langford. A global geometric framework for nonlinear dimensionality reduction. *Science*, 290(5500):2319–2323, 2000. doi: 10.1126/science.290.5500.2319
- [34] C. Thomas and A. Kovashka. Who’s behind the camera? identifying the authorship of a photograph. *CoRR*, abs/1508.05038, 2015.
- [35] W. S. Torgerson. Multidimensional scaling of similarity. *Psychometrika*, 30(4):379–393, Dec 1965. doi: 10.1007/BF02289530
- [36] L. van der Maaten and G. Hinton. Visualizing High-Dimensional Data Using t-SNE. *Journal of Machine Learning Research*, 9:2579–2605, Nov. 2008.
- [37] M. van Kreveld and B. Speckmann. *On Rectangular Cartograms*, pp. 724–735. Springer Berlin Heidelberg, Berlin, Heidelberg, 2004.
- [38] Y. Weiss, A. Torralba, and R. Fergus. Spectral hashing. In D. Koller, D. Schuurmans, Y. Bengio, and L. Bottou, eds., *Advances in Neural Information Processing Systems 21*, pp. 1753–1760. Curran Associates, Inc., 2009.